



OPEN

Photocatalytic efficiency under visible light of a novel Cu–Fe oxide composite films prepared by one-step sparking process

Arisara Panthawan^{1,3}, Nidchamon Jumrus³, Panupong Sanmuangmoon⁴, Winai Thongpan³, Tewasin Kumpika², Wattikon Sroila³, Ekkapong Kantarak³, Adisorn Tuantranont⁵, Pisith Singjai^{2,3,6} & Wiradej Thongsuwan^{2,3,6}✉

Copper–iron (Cu–Fe) oxide composite films were successfully deposited on quartz substrate by a facile sparking process. The nanoparticles were deposited on the substrate after sparking off the Fe and Cu tips with different ratios and were then annealed at different temperatures. The network particles were observed after annealing the film at 700 °C. Meanwhile, XRD, XPS and SAED patterns of the annealed films at 700 °C consisted of a mixed phase of CuO, γ -Fe₂O₃, CuFe₂O₄ and CuFe₂O. The film with the lowest energy band gap (E_g) of 2.56 eV was observed after annealing at 700 °C. Interestingly, the optimum ratio and annealing temperature show the photocatalytic activity under visible light higher than 20% and 30% compare with the annealed TiO₂ at 500 and 700 °C, respectively. This is a novel photocatalyst which can be replaced TiO₂ for photocatalytic applications in the future.

Photocatalysis is a green technology for environmental purification, in particular the decomposition of organic pollutants^{1–3}. Over the last decade, many researchers have been reported that n-type semiconductor materials successfully photodegraded organic pollutants based such as titanium dioxide (TiO₂)^{4–7}. Anywise, n-type semiconductors are still limited due to their large forbidden bands, low quantum yields, and unsuitable conduction band edges^{8,9}. Thus, p-type semiconductors have been developed to expand the field of photocatalysis¹⁰. Copper (Cu) and iron (Fe) oxide are p-type semiconductors that can exhibit much more excellent properties in many applications^{10–13}.

Generally, the combinations of metal oxide can produce a novel compound which might improve their physical, chemical, optical and electrical properties, such as Cu–Fe oxides^{14–17}. However, the report about Cu–Fe oxides in the field of photocatalysis is infrequently found. In this work, we aim to synthesize novel Cu–Fe oxides composite films by a one-step sparking process. This process has been developed in our lab which can prepare small, uniform particles, high porous films, and determine the composite ratio^{18–26}. Moreover, the sparking process requires neither complicated steps nor special equipment, cheap, fast, and non-toxic. Surface morphology, chemical and optical properties of the as-deposited composite films were improved by heat treatment. The effect of heat treatment on morphology, chemical and optical properties were reported and discussed. Furthermore, the photocatalytic activity under visible light between Cu–Fe oxides and TiO₂ films was examined and compared.

Experimental details

The experiment was carried out using a high DC voltage of 2.0 kV applied to Fe tips (0.25 mm, purity 99.5%, Advent Research Material Ltd.), and Cu tips (0.25 mm, purity 99.9%, Advent Research Material Ltd, UK). Cu:Fe with the ratios of 4:0, 3:1, 2:2, 1:3, and 0:4 can be defined from the number of sparking heads. The tips were placed 1.5 cm above the quartz substrate (1 × 1 cm²) at 1 mm spacing under atmospheric pressure. The nanoparticles

¹PhD's Degree Program in Materials, Faculty of Science, and Graduate School in Chiang Mai University (GSCMU), Chiang Mai, Thailand. ²Center of Excellence in Materials Science and Technology, Chiang Mai University, Chiang Mai, Thailand. ³Department of Physics and Materials Science, Faculty of Science, Chiang Mai University, Chiang Mai, Thailand. ⁴Faculty of Science, Chiang Mai University, Chiang Mai, Thailand. ⁵Thailand Organic and Printed Electronics Innovation Center, National Electronics and Computer Technology Center, National Science and Technology Development Agency, Klong Luang 12120, Pathumthani, Thailand. ⁶Research Center in Physics and Astronomy, Faculty of Science, Chiang Mai University, 239, Huay Kaew Road, Muang, Chiang Mai 50200, Thailand. ✉email: wiradej.t@cmu.ac.th

were then deposited on the substrate with a deposition rate of 52.33 nm/min for 10 min after sparking off the Fe and Cu tips. The as-deposited films were then annealed at 500, 600, 700, 800, and 900 °C for 60 min to improve their crystallinity.

Morphology, chemical and optical properties of the samples were characterized using scanning electron microscopy (SEM, JEOL JSM300 and SEM, JEOL JSM 6335F), transmission electron microscopy (TEM, JEOL JEM 2010), X-ray Photoelectron Spectroscopy (XPS, AXIS Ultra DLD-X-ray Photoelectron Spectrometer and a monochromatic AlK α X-ray excitation source) and UV–Vis spectroscopy (Hitachi U-4100).

Photocatalytic activity under visible light was investigated by the decomposition of methylene blue (MB) solution (Ajax Finechem). The samples were dipped into 3.0 mL of MB solution with a concentration of 10.0 μ M and then irradiated a lamp (TB814SU-Y lamp with wavelength and luminance of 340–900 nm and 6.57×10^5 Lux, respectively) for 1–5 h. Degradation of MB can be indicated by measuring the absorbance using UV–Vis spectrophotometer.

Results and discussion

The mass loading of the TiO $_2$ and Cu–Fe composite photocatalyst on quartz substrates in this work was 0.12 mg/10 min. This result is in good agreement with our previous papers^{26,27}. The effect of Cu:Fe ratio and annealing temperature on MB degradation have shown in Fig. 1a,b. Moreover, the annealed TiO $_2$ at 500 °C and 700 °C which were prepared by the sparking process were used to compare MB degradation with the Cu–Fe oxide film at 700 °C against irradiation time, as shown in Fig. 1c. It is noted that the annealed Cu–Fe oxide film at 700 °C with the ratio of 2:2 has a degradation performance higher than 20–30% compared with the well-known photocatalyst such as TiO $_2$. Thus, a new finding of Cu–Fe oxide which was used as photocatalyst is a strong point of this work.

Figure 2a shows the morphology of the annealed Cu–Fe oxide film at 700 °C with a ratio of 2:2. The nanoparticles were aligned to networks with the length and width of 1410 nm and 279 nm. This is because of the high surface energy of nanoparticles, Cu–Fe oxide nanoclusters were agglomerated to decrease their surface energy. Meanwhile, the agglomeration of adjoining grains becomes more observable for higher kinetic energy^{28,29}. According to the arrangement of the network particles, it can increase the MB decomposition which corresponds to Fig. 1b.

TEM image of the annealed Cu–Fe oxide film at 700 °C with a ratio of 2:2 is shown in Fig. 2b. It is clearly seen that the actual particle sizes are in the range of 4–15 nm, while the energy dispersive x-ray shows the amount of Cu, Fe, and O are 28.26, 31.44, and 40.35 atomic %, respectively (data not shown). Moreover, the selected area electron diffraction (SAED) (inset) shows well-established diffraction rings matching most closely with CuO in the (111), (002) plane (JCPDS 48-0937), γ -Fe $_2$ O $_3$ in the (311), (220), (400) planes (JCPDS 39-1346), CuFe $_2$ O $_4$ in the (101), (211), (220), (224) planes (JCPDS 34-0425), and CuFeO $_4$ in the (006), (012), (018) plane (JCPDS 39-0246). Morphology of the annealed TiO $_2$ film at 500 °C is shown in Fig. 2c. The mass loading of \sim 0.12 mg/10 min was obtained on the quartz substrate. The primary nanoparticles were agglomerated to form network particles.

Figure 3a shows XRD patterns of the annealed Cu–Fe composite films at 700 °C with various Cu:Fe ratios. It is noted that the ratio has a direct effect on the quantity of each composite film. Interestingly, the ratio of 2:2 shows many Cu–Fe phase compositions which have the highest photocatalytic activity (see Fig. 1a). It might occur the mix-phases can enhance the electronic and optical properties of the films. Figure 3b shows the Cu–Fe composite films with a ratio of 2:2 at different annealing temperatures. No significant peak was observed at the annealed films lower than 600 °C. At 700 °C, the peaks of 30.08° and 35.52° correspond to the (220) and (211) crystal planes of the CuFe $_2$ O $_4$. The peak of $2\theta = 35.72^\circ$ was the (012) crystal planes of the CuFeO $_2$. The peaks at 35.56° and 38.77° were the (002) and (111) crystal planes of the CuO. And, the peaks at 35.61° and 43.5° correspond to the (311) and (400) crystal planes of the γ -Fe $_2$ O $_3$. However, the peak at 35° consisted of CuO, γ -Fe $_2$ O $_3$, CuFe $_2$ O $_4$ and CuFe $_2$ O. While the peaks of anatase and rutile TiO $_2$ were observed at 25°, 48° and 27.5°, 55° in the annealed film at 500 °C²² (show in Fig. 3c).

XPS spectra of the annealed Cu–Fe oxide composite films at 500, 600, 700, 800, and 900 °C for 1 h are shown in Fig. 4. Figure 4a shows symmetric peaks at binding energies of 932.5–934.5 eV and 953.5–954.2 eV assigned to the Cu 2p $_{3/2}$ and Cu 2p $_{1/2}$, respectively. From the figure, the binding energy of 933.7 eV³⁰ which corresponds to CuFe $_2$ O $_4$ shows a strong peak after annealing at 700 °C. Whereas the smaller peaks consist of CuO (934.2 eV)³¹ and CuFeO $_2$ (932.6 eV)³².

The two peaks at 710.5–712.8 eV and 724.5–726.8 eV attributed to Fe 2p $_{3/2}$ and Fe 2p $_{1/2}$ which are characteristic of Fe ions in Cu–Fe oxide films. After the film annealing at 700 °C, the highest peak assigned to CuFeO $_2$ at 710.6 eV³³. Moreover, two smaller peaks located at 711.2³⁴ and 712.8 eV³⁵ corresponds to γ -Fe $_2$ O $_3$ and CuFe $_2$ O $_4$, respectively.

Figure 4c shows the O 1s spectra at various annealing temperatures which can be deconvoluted into three peaks at 532.9³⁶, 531.1³⁷, and 530.2 eV³⁸, which correspond to SiO $_2$, Cu(OH) $_2$, and Fe(OH)O, respectively. However, the peak of SiO $_2$ (532.9 eV) increased with increasing the annealing temperature. This is due to the agglomeration of network particles at a high temperature can increase the quartz substrate spacing, which corresponds to the SEM result (see Fig. 2a).

The effect of the annealing temperature on the phase transformation can be evaluated by XPS (shown in Fig. 4) are shown in Fig. 4d. It is noted that the CuFe $_2$ O $_4$ and CuFeO $_2$ were increased with increasing the annealing temperature³⁹. However, an exceed CuFeO $_2$ at the annealing temperature higher than 700 °C might inhibit the photocatalytic reactions. This is due to the factors causing the thin films to have an increased energy gap when the temperature is higher than 700 °C because of the effects of % rate of the crystal structure, microstructure characteristics, and the characteristics of chemical compositions¹³.

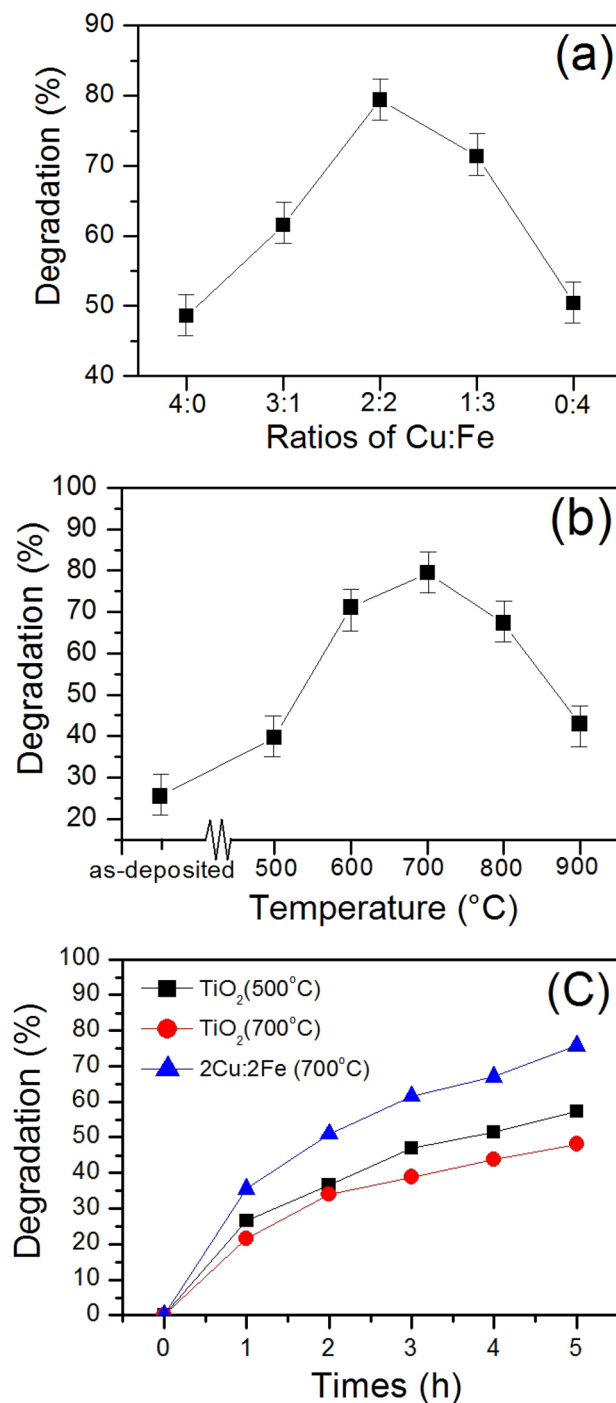


Figure 1. plot of degradation versus (a) ratios of Cu:Fe, (b) annealing temperatures, (c) irradiation time of the Cu-Fe oxide films.

Figure 5 shows the energy band gap (E_g) of the as-deposited, the annealed Cu-Fe oxide films at 500, 600, 700, 800 and 900 °C which are 5.35 eV, 3.88 eV, 2.89 eV, 2.56 eV, 2.94 eV and 5.63 eV, respectively. This behavior can be described by an atom distancing increased with the increasing of annealing temperature⁴⁰. Interestingly, the annealing at 700 °C not only shows the lowest E_g but also shows the highest photocatalytic activity (see Fig. 2b). This is because of the good mixing ratio between Cu and Fe oxide phases⁴¹.

Increasing of photocatalytic activity in the annealed Cu-Fe oxide film at 700 °C with a ratio of 2:2 can be described by Cu-Fe mixed-phase mechanism, as shown in Fig. 6. The generation of photocatalytic mechanism is based on pairs of electrons (e^-) and holes (h^+) over the composites⁴². The E_{VB} of CuO, γ -Fe₂O₃, CuFe₂O₄, and CuFeO₂ are +2.10, +2.67, +2.06, and +2.46 eV/NHE. While, the E_{CB} of CuO, γ -Fe₂O₃, CuFe₂O₄, and CuFeO₂ are +0.52, +0.09, +0.64 and -0.14 eV/NHE, it can be theoretically calculated using the empirical formula⁴³. The

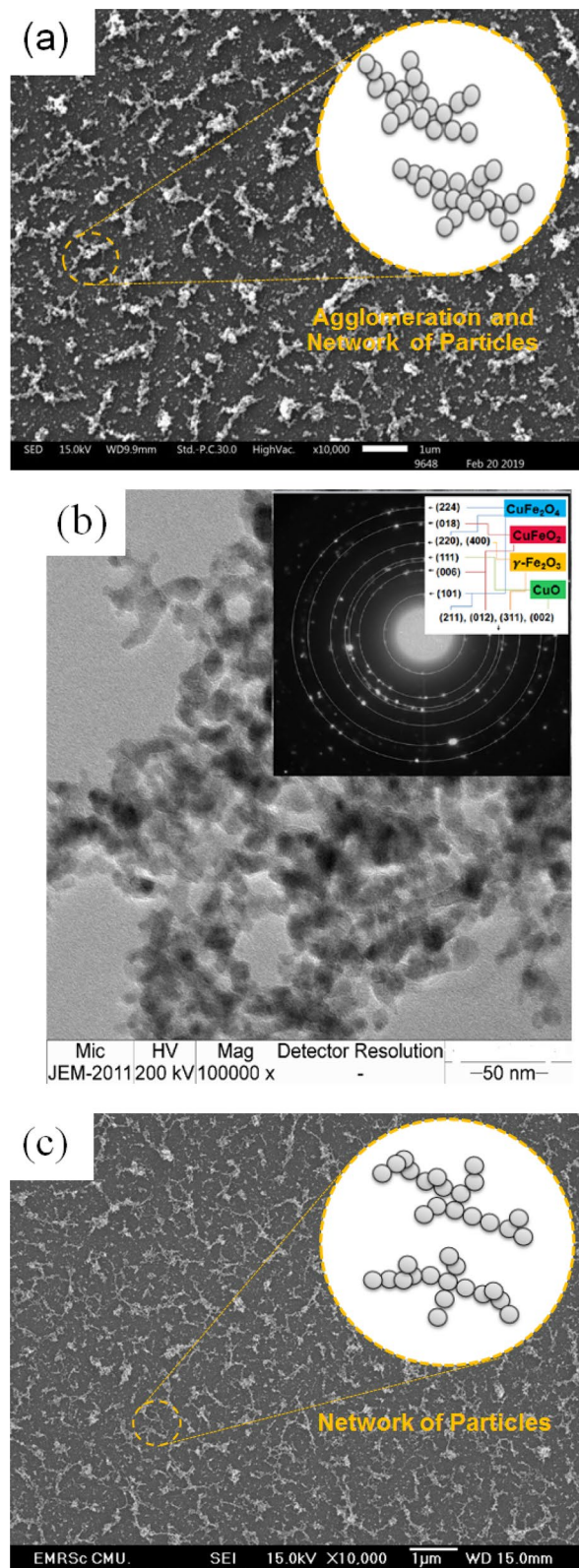


Figure 2. (a) SEM image, (b) TEM image and their SAED pattern (inset) of the annealed Cu–Fe oxide film at 700 °C with a ratio of 2:2 and (c) SEM image of the annealed TiO₂ film at 500 °C.

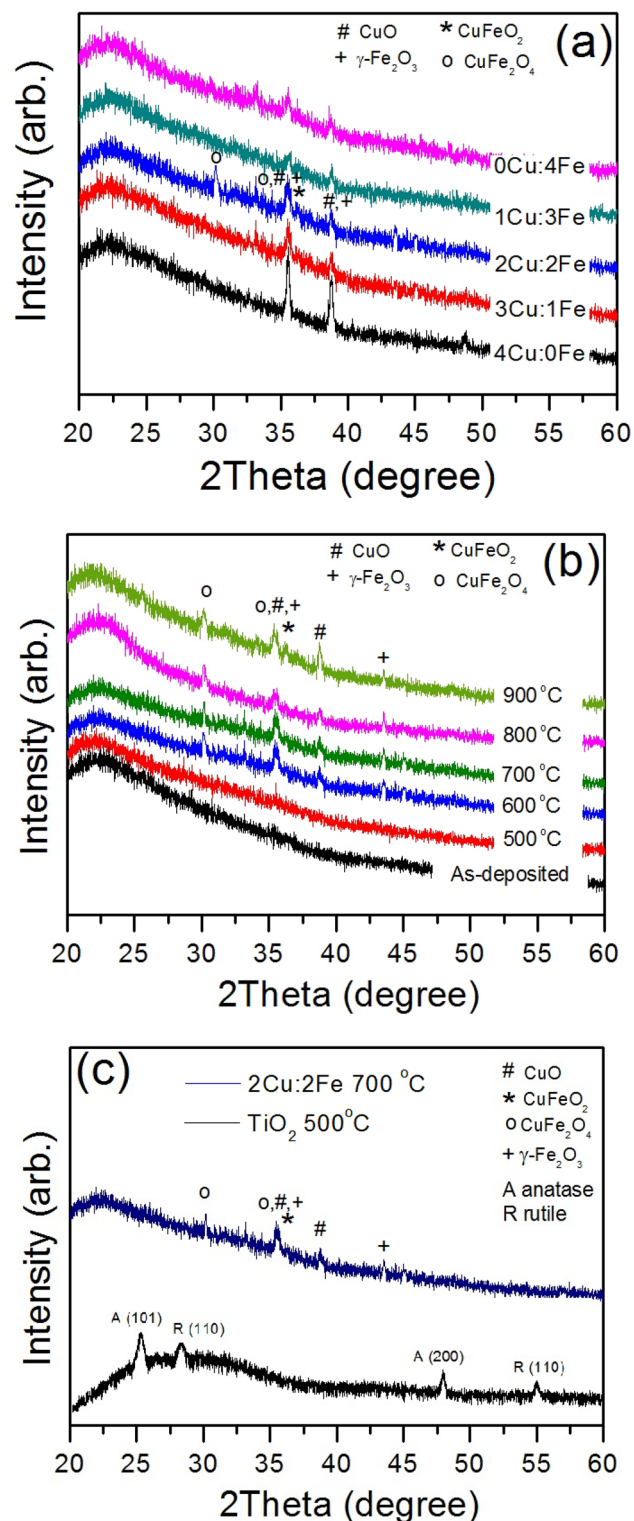


Figure 3. XRD patterns of (a) the annealed films at 700 °C with different Cu:Fe ratios, (b) the annealed Cu–Fe films with a ratio of 2:2 at different annealing temperatures and (c) the Cu–Fe films with optimum ratio and annealing temperature compare with the annealed TiO₂ film at 500 °C.

possible photocatalytic mechanism of the optimum condition was started by photo-generated electrons (e^-) and holes (h^+) pairs from CuFe₂O₄ and CuO. The photo-excited e^- in the γ -Fe₂O₃ and CuFeO₂ were injected into the CB of the CuFe₂O₄ and CuO. While, the photo-excited h^+ would transfer to the surface of γ -Fe₂O₃ and

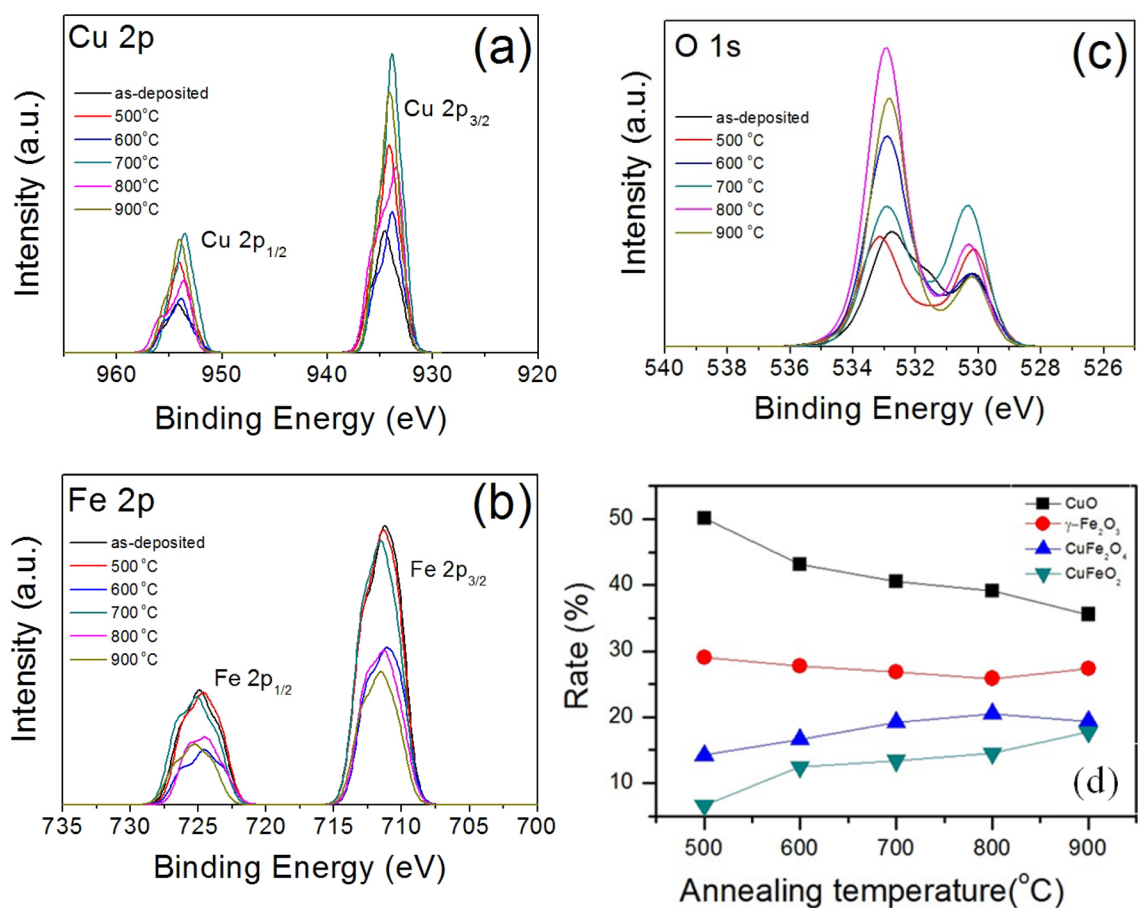


Figure 4. XPS spectra of the Cu–Fe oxide films with different Cu:Fe ratios and annealing temperatures: (a) Cu 2p, (b) Fe 2p, (c) O 1s, and (d) comparison of the Cu–Fe phases at different annealing temperatures.

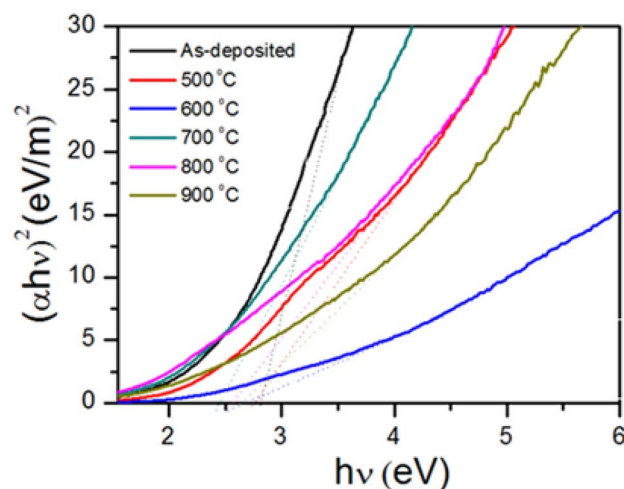


Figure 5. plot of $(\alpha h\nu)^2$ versus photon energy of the films at different annealing temperatures.

CuFeO₂, which can improve the charge separation and inhibit the e^-/h^+ recombination. This is a key factor for the enhancing photocatalytic activity of the annealed Cu–Fe oxide film at 700 °C with a ratio of 2:2 which is greater than a photocatalyst as TiO₂.

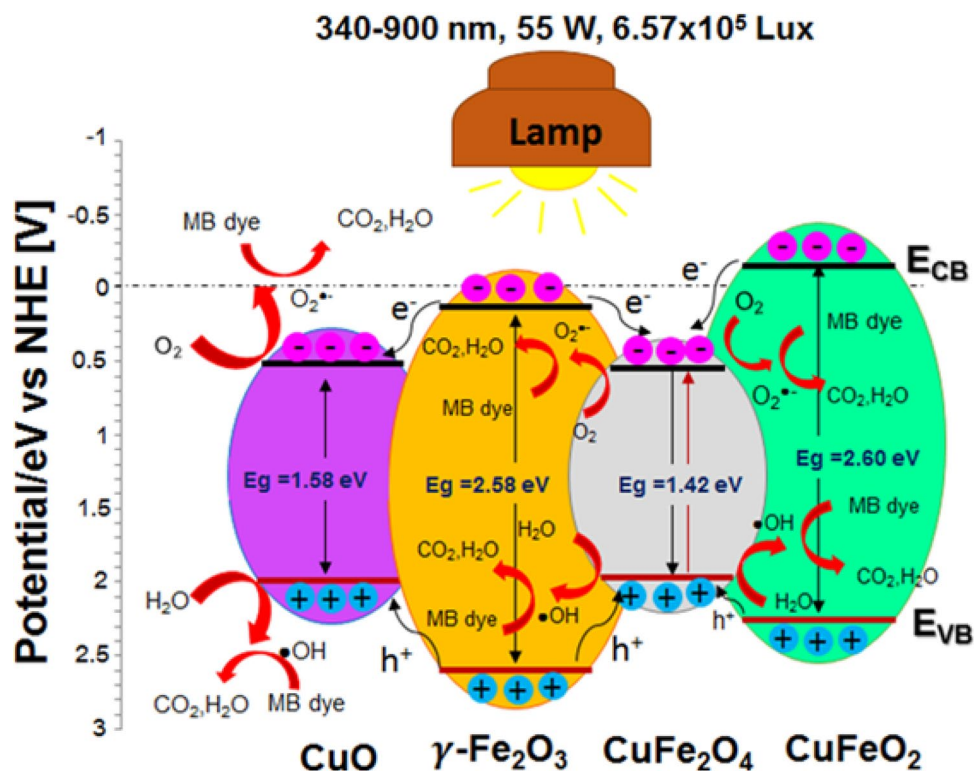


Figure 6. schematic diagram for photocatalytic mechanism of the optimum condition.

Conclusions

A novel photocatalyst Cu–Fe oxide films were successfully prepared by a one-step sparking process. The Cu:Fe ratio and annealing temperature are play important role in the photocatalytic efficiency of the Cu–Fe oxide films. This work concluded that the optimum ratio of Cu:Fe and annealing temperature for MB degradation were 2:2 and 700 °C. Moreover, the optimum condition has the photocatalytic efficiency higher than the annealed TiO₂ at 500 and 700 °C for 20% and 30%, respectively. The results show the Cu:Fe ratio has a direct effect on photocatalytic activity. Furthermore, the annealing temperature not only affects the surface morphology but also affects the E_g and photocatalytic activity. A new finding of this work is the higher performance photocatalyst than TiO₂ which can be developed and used for photocatalytic applications in the future.

Received: 17 December 2021; Accepted: 3 March 2022

Published online: 10 March 2022

References

- Herrmann, J.-M. *et al.* Environmental Green Chemistry as defined by photocatalysis. *J. Hazard. Mater.* **146**, 624–629. <https://doi.org/10.1016/j.jhazmat.2007.04.095> (2007).
- Saitow, K., Wang, Y. & Takahashi, S. Mechano-synthesized orange TiO₂ shows significant photocatalysis under visible light. *Sci. Rep.* **8**, 15549. <https://doi.org/10.1016/j.cej.2015.10.112> (2018).
- Chen, M. *et al.* Nanofiber template-induced preparation of ZnO nanocrystal and its application in photocatalysis. *Sci. Rep.* **11**, 21196 (2021).
- Rani, M. & Shanker, U. Green synthesis of TiO₂ and its photocatalytic activity. In *Hand book of Smart Photocatalytic Materials* 11–61 (2020). <https://doi.org/10.1007/s10854-015-2832-7>.
- Thongsuwan, W., Kumpika, T. & Singjai, P. Effect of high roughness on a long aging time of superhydrophilic TiO₂ nanoparticle thin films. *Curr. Appl. Phys.* **11**, 1237–1242. <https://doi.org/10.1016/j.cap.2011.03.002> (2011).
- Gherbi, R., Nasrallah, N., Amrane, A., Maachi, R. & Trari, M. Photocatalytic reduction of Cr(VI) on the new hetero-system CuAl₂O₄/TiO₂. *J. Hazard. Mater.* **186**, 1124–1130. <https://doi.org/10.1016/j.jhazmat.2010.11.105> (2011).
- Hankhantod, A. *et al.* External electric and magnetic fields enhanced photocatalytic efficiency of TiO₂ nanoparticulate films prepared by sparking process. *Mater. Lett.* **300**, 130147. <https://doi.org/10.1016/j.matlet.2021.130147> (2021).
- Nowotny, M. K. *et al.* Observations of p-type semiconductivity in titanium dioxide at room temperature. *Mater. Lett.* **64**, 928–930. <https://doi.org/10.1016/j.matlet.2010.01.061> (2010).
- Derbar, A., Omeiri, S., Bouguelia, A. & Trai, M. Characterization of new heterosystem CuFeO₂/SnO₂ application to visible-light induced hydrogen evolution. *Int. J. Hydrogen Energy* **33**, 4274–4282. <https://doi.org/10.1016/j.ijhydene.2008.05.067> (2008).
- Reag, C. G., Park, Y. & Choi, K.-S. Electrochemical synthesis of p-type CuFeO₂ electrodes for use in a photoelectrochemical cell. *J. Phys. Chem. Lett.* **3**, 1872–1876. <https://doi.org/10.1021/jz300709t> (2012).
- Xu, Q., Li, R., Li, R., Wang, C. & Yuan, D. Visible-light photocatalytic reduction of Cr(VI) using nano-sized delafossite (CuFeO₂) synthesized by hydrothermal method. *J. Alloys Compd.* **723**, 441–447. <https://doi.org/10.1016/j.jallcom.2017.06.243> (2017).
- Bassaïd, S., Chaib, M., Omeiri, S., Bouguelia, A. & Trari, M. Photocatalytic reduction of cadmium over CuFeO₂ synthesized by sol-gel. *J. Photochem. Photobiol. A Chem.* **201**, 62–68. <https://doi.org/10.1016/j.jphotochem.2008.09.015> (2009).

13. Yu, R.-S., Lee, Y.-F. & Lai, Y.-S. Synthesis and optoelectronic properties of CuFeO₂ semiconductor thin films. *ECS J. Solid State Sci. Technol.* **5**, 646–652. <https://doi.org/10.1149/2.0091612jss> (2016).
14. Liu, Q.-L., Zhao, Z.-Y., Zhao, R.-D. & Yi, J.-H. Fundamental properties of delafossite CuFeO₂ as photocatalyst for solar energy conversion. *J. Alloys Compd.* **819**, 153032. <https://doi.org/10.1016/j.jallcom.2019.153032> (2019).
15. Jiang, T., Xu, C., Zhang, Y., Zhang, Y. & Tian, J. Wet chemical epitaxial growth of cactus-like CuFeO₂/ZnO heterojunction for improved photocatalysis. *Dalton Trans.* **49**, 9574–9578. <https://doi.org/10.1039/D0DT01813A> (2020).
16. Tamaddon, F., Nasiri, A. & Yazdanpanah, G. Photocatalytic degradation of ciprofloxacin using CuFe₂O₄@methyl cellulose based magnetic nanobiocomposite. *MethodsX* **7**, 74–81. <https://doi.org/10.1016/j.mex.2019.12.005> (2020).
17. Yang, H., Yan, J., Lu, Z., Cheng, X. & Tang, Y. Photocatalytic activity evaluation of tetragonal CuFe₂O₄ nanoparticles for the H₂ evolution under visible light irradiation. *J. Alloys Compd.* **476**, 715–719. <https://doi.org/10.1016/j.jallcom.2008.09.104> (2009).
18. Chuminjak, Y. *et al.* Electrochemical energy-storage performances of nickel oxide films prepared by a sparking method. *RSC Adv.* **5**, 67795. <https://doi.org/10.1039/c5ra09408a> (2015).
19. Hankhntod, A. *et al.* α-Fe₂O₃ modified TiO₂ nanoparticle films prepared by sparking off Fe electroplated Ti tips. *Appl. Surf. Sci.* **477**, 116–120. <https://doi.org/10.1016/j.apsusc.2017.11.224> (2019).
20. Louloudakis, D. *et al.* Novel spark method for deposition of metal oxide thin films: Deposition of hexagonal tungsten oxide. *Phys. Status Solidi A Appl. Mater. Sci.* **216**, 1970028. <https://doi.org/10.1002/pssa.201970028> (2019).
21. Thongpan, W. *et al.* Electrochromic properties of tungsten oxide films prepared by sparking method using external electric field. *Thin Solid Films* **682**, 135–141. <https://doi.org/10.1016/j.tsf.2019.04.010> (2019).
22. Panthawan, A. *et al.* Hot air treatment: Alternative annealing of TiO₂ nanoparticle films without substrate deformation. *AIP Conf. Proc.* **2279**, 120003. <https://doi.org/10.1063/5.0024035> (2020).
23. Panthawan, A. *et al.* Photocatalytic enhancement of a novel composite CuAl₂O₄/TiO₂/CuO films prepared by sparking process. *Opt. Int. J. Light Electron Opt.* **224**, 165502. <https://doi.org/10.1016/j.jijleo.2020.165502> (2020).
24. Tippo, P. *et al.* Influence of Co concentration on properties of NiO film by sparking under uniform magnetic field. *Sci. Rep.* **10**, 15690. <https://doi.org/10.1038/s41598-020-72883-x> (2020).
25. Rućman, S. *et al.* Influence of the magnetic field on bandgap and chemical composition of zinc thin films prepared by sparking discharge process. *Sci. Rep.* **10**, 1388. <https://doi.org/10.1038/s41598-020-58183-4> (2020).
26. Thongsuwan, W., Kumpika, T. & Singjai, P. Photocatalytic property of colloidal TiO₂ nanoparticles prepared by sparking process. *Curr. Appl. Phys.* **8**, 563–568. <https://doi.org/10.1016/j.cap.2007.10.004> (2008).
27. Thongpan, W. *et al.* External-electric-field-enhanced uniformity and deposition rate of a TiO₂ film prepared by the sparking process. *Ukr. J. Phys.* **63**, 6. <https://doi.org/10.15407/ujpe63.6.531> (2018).
28. Panthawan, A. *et al.* Morphology and phase transformation of copper/aluminium oxide films. *Ukr. J. Phys.* **63**, 425. <https://doi.org/10.15407/ujpe63.5.425> (2018).
29. Seipenbusch, M., Toneva, P., Peukert, W. & Weber, A. P. Impact fragmentation of metal nanoparticle agglomerates. *Part. Part. Syst. Charact.* **24**, 193–200. <https://doi.org/10.1002/ppsc.200601089> (2007).
30. McIntyre, N. S. & Cook, M. G. X-ray photoelectron studies on some oxides and hydroxides of cobalt, nickel, and copper. *Anal. Chem.* **47**, 2208 (1975).
31. Capece, F. M. *et al.* “Copper chromite” catalysts: XPS structure elucidation and correlation with catalytic activity. *J. Electron Spectrosc. Relat. Phenom.* **27**, 119–128. [https://doi.org/10.1016/0368-2048\(82\)85058-5](https://doi.org/10.1016/0368-2048(82)85058-5) (1982).
32. Kim, J.-H., Kim, J., Choi, Y. H. & Youn, D. H. Facile CuFeO₂ microcrystal synthesis for lithium ion battery anodes via microwave heating. *J. Mater. Sci. Mater. Electron.* **31**, 12. <https://doi.org/10.1007/s10854-020-03480-x> (2020).
33. Xiong, D. *et al.* Hydrothermal synthesis of delafossite CuFeO₂ crystals at 100 degrees C. *RSC Adv.* **5**, 61. <https://doi.org/10.1039/C5RA08227G> (2015).
34. Oku, M. & Hirokawa, K. XPS of Co₃O₄, Fe₃O₄, Mn₂O₄ and related compounds. *J. Electron Spectrosc. Relat. Phenom.* **8**, 475 (1976).
35. Li, X. *et al.* High performance of manganese porphyrin sensitized p-type CuFe₂O₄ photocathode for solar water splitting to produce hydrogen in a tandem photoelectrochemical cell. *Catalysts* **8**(3), 108. <https://doi.org/10.3390/catal8030108> (2018).
36. Iimura, K., Suzuki, N. & Kato, K. Syntheses of highly ordered mesoporous materials, FSM-16, derived from kanemite. *Bull. Chem. Soc. Jpn.* **69**, 1201. <https://doi.org/10.1246/bcsj.69.1449> (1996).
37. McIntyre, N. S., Sunder, S., Shoesmith, D. W. & Stanchell, F. W. Chemical information from XPS-applications to the analysis of electrode surfaces. *J. Vac. Sci. Technol.* **18**, 714. <https://doi.org/10.1116/1.570934> (1981).
38. McIntyre, N. S. & Zetaruk, D. G. X-ray photoelectron spectroscopic studies of iron oxides. *Anal. Chem.* **49**, 1521–1529. <https://doi.org/10.1021/ac50019a016> (1977).
39. Jbara, H. B. *et al.* Preparation of Cu–Fe–O thin films via post oxidation of iron/copper bilayers: structural, optical and electrical properties. *Opt. Quantum Electron.* <https://doi.org/10.1007/s11082-019-1807-y> (2019).
40. O'Donnell, K. P. & Chen, X. Temperature dependence of semiconductor band gaps. *Appl. Phys. Lett.* **58**, 2924–2926. <https://doi.org/10.1063/1.104723> (1991).
41. Bera, A., Deb, K., Chattopadhyay, K. K., Thapa, R. & Saha, B. Mixed phase delafossite structured p type CuFeO₂/CuO thin film on FTO coated glass and its Schottky diode characteristics. *Microelectron. Eng.* **162**, 23–26. <https://doi.org/10.1016/j.mee.2016.04.020> (2016).
42. Karthikeyan, N., Narayanan, V. & Stephen, A. Degradation of textile effluent using nanocomposite TiO₂/SnO₂ semiconductor photocatalysts. *Int. J. ChemTech Res.* **8**, 443–449 (2015).
43. Mousavi, M., Habibi-Yangjeh, A. & Abitorabi, M. Fabrication of novel magnetically separable nanocomposites using graphitic carbon nitride, silver phosphate and silver chloride and their applications in photocatalytic removal of different pollutants using visible-light irradiation. *J. Colloid Interface Sci.* **480**, 218–231. <https://doi.org/10.1016/j.jcis.2016.07.021> (2016).

Acknowledgements

The authors are thankful to the Thailand Graduate Institute of Science and Technology (TGIST) (SCA-CO-2560-4484-TH, TG-44-10-60-023D), the National Science and Technology Development Agency (NSTDA), and the Graduate School Department of Physics and Materials Science, Faculty of Science, Chiang Mai University (GSCMU) for their generous financial support. And, this research work was partially supported by Chiang Mai University.

Author contributions

A.P.: Investigation, Validation, Visualization, Writing-Original Draft, Writing, Review & Editing (Revision). W.T.: Methodology, Validation, Resources, Writing-Original Draft. T.K.: Methodology, Validation, Resources, Writing-Original Draft. N.J.: Methodology, Validation, Resources, Writing-Original Draft. P.S.: Methodology, Validation, Resources, Writing-Original Draft. W.S.: Methodology, Validation, Resources, Writing-Original Draft. E.K.: Methodology, Validation, Resources, Writing-Original Draft. A.T.: Methodology, Validation, Resources,

Writing-Original Draft.P.S.: Methodology, Validation, Resources, Writing-Original Draft.W.T.: Conceptualization, Methodology, Validation, Resources, Writing, Supervision, Review & Editing (Revision).

Competing interests

The authors declare no competing interests.

Additional information

Correspondence and requests for materials should be addressed to W.T.

Reprints and permissions information is available at www.nature.com/reprints.

Publisher's note Springer Nature remains neutral with regard to jurisdictional claims in published maps and institutional affiliations.



Open Access This article is licensed under a Creative Commons Attribution 4.0 International License, which permits use, sharing, adaptation, distribution and reproduction in any medium or format, as long as you give appropriate credit to the original author(s) and the source, provide a link to the Creative Commons licence, and indicate if changes were made. The images or other third party material in this article are included in the article's Creative Commons licence, unless indicated otherwise in a credit line to the material. If material is not included in the article's Creative Commons licence and your intended use is not permitted by statutory regulation or exceeds the permitted use, you will need to obtain permission directly from the copyright holder. To view a copy of this licence, visit <http://creativecommons.org/licenses/by/4.0/>.

© The Author(s) 2022